Trapping forces in a multiple-beam fiber-optic trap

Erkin Sidick, Scott D. Collins, and André Knoesen

Transverse and axial trapping forces are calculated in the ray optics regime for a multiple-beam fiber-optic light-force trap for dielectric microspheres located both on and off axis relative to the beam axis. Trap efficiencies are evaluated as functions of the effective index of refraction of the microspheres, normalized sphere radius, and normalized beam waist separation distance. Effects of the linear polarization of the electric field and of beam focusing through microlenses are considered. In the case of a counterpropagating two-beam fiber-optic trap, using microlenses at the distal ends of the fiber to focus the beams may somewhat increase the trapping volume and the axial stability if the fiber spacing is sufficiently large but will greatly reduce the stiffness of the transverse force. Trapping forces produced in a counterpropagating two-beam fiber-optic trap are compared with those generated in multiple-beam fiber-optic gradient-force traps. Multiple-beam fiber-optic traps use strong gradient forces to trap a particle; therefore they stabilize the particles much more firmly than do counterpropagating two-beam traps.

Key words: Fiber-optic trap, laser trap, optical tweezers, radiation pressure.

1. Introduction

Optical trapping is a technique that is used to capture, translate, and manipulate microscopic particles, such as dielectric microspheres, cells, oglio cell organisms, and cell organelles. In an optical trap refraction and reflection of light give rise to two different types of force on the particle. Refraction gives rise to a gradient force, which is due to an optical intensity gradient and points toward the direction of increased optical intensity. Reflection gives rise to a scattering force, or radiation pressure, which is proportional to the optical intensity and points in the direction of light propagation.

The first optical trap was demonstrated by Ashkin[1] using two counterpropagating, coaxially aligned laser beams to trap dielectric spheres suspended in liquid. In this dual-beam approach, the particle is confined to the common beam axis by the transverse gradient forces of the two weakly focused laser beams. The particle is stabilized axially at a location where the scattering forces of the two beams balance each other. The relative trap position on the axis of the beams can be easily adjusted by changing the relative intensities of the two laser beams. Later Ashkin and coworkers demonstrated another optical trap, using a single beam,[2] which is called a single-beam gradient trap or optical tweezers. In the single-beam gradient-force trap the beam is strongly focused to a diffraction-limited spot by a high-numerical-aperture objective. A strong three-dimensional gradient-force trap is created at the bright focus of the beam. Weaker scattering forces push the particle slightly below the focus.

Recently a new version of dual-beam optical traps was demonstrated with optical fibers.[3] The fiber-optic trap is created by the beams emerging from two coaxially aligned optical fibers. As compared with other embodiments, this implementation is most economical, much simpler to operate, and requires relatively low optical power to capture particles effectively in a range of dimensions, as is discussed in detail in Refs. 3 and 4. A common drawback of this and the conventional counterpropagating two-beam traps is the weak confinement of the particle in the longitudinal direction by the combined, weak scattering force of the two beams. However, as we show in this paper, one can construct a multiple-beam fiber-optic, gradient-force trap in which only gradient forces are used to stabilize the particle in three dimensions. For example, when four fibers are placed on a common plane with their beams forming a cross

When the research was done the authors were with the Department of Electrical Engineering, University of California, Davis, California 95616. E. Sidick is now with CVI Laser Corporation, 361 Lindbergh Avenue, Livermore, California 94550.

Received 16 May 1996; revised manuscript received 9 December 1996.

0003-6935/97/256423-11$10.00/0

hair at the beam center, the beams produce a strong gradient-force field at the beam center and can firmly trap a particle. The gradient forces produced by the beams of only two or three adjacent fibers can also strongly confine a particle in three dimensions.

Theoretical analysis plays an important role in estimating the strength of the forces produced in an optical trap and in understanding the differences of the different types of optical traps. Although optical traps are ultimately used to capture and to manipulate micro-organisms and cells having irregular shapes, to simplify the analysis they are usually characterized with a spherical dielectric particle assumed to be the object to be trapped. Depending on the relationship of the diameter $2r_o$ of the particle and the free-space wavelength λ_o of the optical beam, the analysis can be divided into three regimes. They are the Rayleigh regime ($2r_o \ll \lambda_o$), the Mie regime ($2r_o \gg \lambda_o$), and the intermediate regime ($2r_o \sim \lambda_o$). In the Mie regime trapping forces can be accurately predicted with the ray optics approximation. The earlier detailed force calculations in the ray optics regime were described by Roosen and co-workers.[5–7] In their analysis the possibility of off-axis location of the sphere relative to the symmetry axis of the laser beam is addressed, but the beam divergence is not taken into account. In other similar analyses following those mentioned above, either the trapping forces are calculated for a tightly focused single-beam gradient force trap[8] or the formulation of the transverse force is not reported[9] or not completely formulated.[10] A complete analysis has not been reported that describes both the axial and the transverse forces produced in a multiple-beam fiber-optic light-force trap, although such an analysis was recently used to predict theoretically the forces produced in a counterpropagating dual-beam fiber-optic trap.[11]

In this paper we calculate, using a formulation based on the ray optics approximation analysis similar to those given in Refs. 8–10, the axial and the transverse forces on spherical microparticles for multiple-beam light-force traps. We evaluate the performance of multiple-beam fiber-optic traps by calculating the forces for a wide range of physical parameters typical for dielectric particles in the Mie regime. We investigate the effects of polarization, the on- and off-axis location of the microparticle, and the divergence of the beam and compare the performance of cleaved-fiber traps with that of lensed-fiber traps. We also compare the performance of dual-beam fiber-optic traps with that of fiber-optic gradient-force traps.

The paper is organized as follows. In Section 2 the axial and the transverse forces of a dual-beam optical trap are derived. The results for a sphere that is not centered on the beam axis are first obtained, then they are simplified for a case where the sphere is centered on the beam axis. A simple, approximate result of the axial force is also provided that is applicable to fiber-optic trapping with a large beam waist separation relative to the value of the beam waist. Numerical analysis of fiber-optic traps is provided in Section 3. Finally, the paper is concluded with some discussions in Section 4.

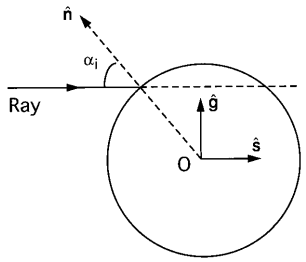

Fig. 1. Gradient and scattering forces exerted by a single ray on a dielectric sphere when the sphere is optically more dense than the surrounding medium: $\hat{\mathbf{n}}$, $\hat{\mathbf{g}}$, and $\hat{\mathbf{s}}$, the unit vectors in the direction of the surface normal, the gradient force, and the scattering force, respectively; α_i, angle of incidence.

2. Formulation of the Problem

Consider a lossless dielectric microsphere illuminated in a nonabsorbing medium by a Gaussian beam with a beam waist (minimum beam radius) of w_o. When a ray strikes a small region of the surface of the microsphere, the force generated by this ray on the microsphere can be decomposed into a scattering-force component $d\mathbf{F}_s$ and a gradient-force component $d\mathbf{F}_g$, which are given by

$$d\mathbf{F}_s = \hat{\mathbf{s}} \frac{n_1}{c} q_s dP, \tag{1a}$$

$$d\mathbf{F}_g = \hat{\mathbf{g}} \frac{n_1}{c} q_g dP, \tag{1b}$$

where n_1 is the refractive index of the medium surrounding the microsphere, dP is the differential power of the ray, c is the free-space light speed, and $\hat{\mathbf{s}}$ and $\hat{\mathbf{g}}$ are the unit vectors in the directions of $d\mathbf{F}_s$ and $d\mathbf{F}_g$, respectively. The relationship of $\hat{\mathbf{s}}$ and $\hat{\mathbf{g}}$ with surface normal $\hat{\mathbf{n}}$ is shown in Fig. 1. In the above equations, q_s and q_g are related to the fractions of the momentum transferred to the microsphere by the emergent rays in the direction parallel to the incident ray q_s and perpendicular to the incident ray q_g, respectively. They are given by[5,6,8,12]

$$q_s = 1 + R \cos 2\alpha_i - T^2 \frac{\cos(2\alpha_i - 2\alpha_r) + R \cos 2\alpha_i}{1 + R^2 + 2R \cos 2\alpha_r}, \tag{2a}$$

$$q_g = -R \sin 2\alpha_i + T^2 \frac{\sin(2\alpha_i - 2\alpha_r) + R \sin 2\alpha_i}{1 + R^2 + 2R \cos 2\alpha_r}, \tag{2b}$$

in which α_i and α_r are angles of incidence and refraction and R and T are the reflectance and transmittance at the surface of the microsphere. Note that these forces are polarization dependent, since both R and T are different for the polarization parallel and perpendicular to the plane of incidence. The effects of polarization are addressed in Subsection 2.A. For

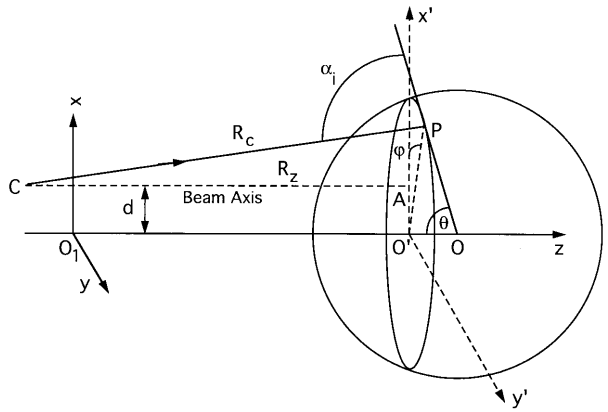

Fig. 2. Geometry of a dielectric sphere hit at point P by a ray coming from a source at point C. The beam waist is located in the xy plane. The beam axis $\overline{CA}$ is away from the z axis by a distance d along the x axis. $\pi - \theta$ and φ are the polar and azimuthal angles, respectively.

a Gaussian beam, the differential power of the beam flowing through a small region of the surface is given by

$$dP = I \cos\theta \, dS = \frac{2P_o}{\pi w_o^2} \exp(-2r^2/w^2) \cos\theta \, dS, \quad (3)$$

where I is the light intensity, P_o is the total power transmitted by the beam, w is the beam radius, dS is a differential surface area on the illuminated part of the microsphere, r is the distance from the beam axis to dS, and θ is the angle between the normal of the differential area dS and the beam axis.[13] The total axial and transverse forces acting on the microsphere can be calculated by integration of the projections of $d\mathbf{F}_s$ and $d\mathbf{F}_g$ on the axial and the transverse directions over the entire surface area that is illuminated by the incident beam. In what follows we first formulate the forces for the general case in which the sphere center is arbitrarily positioned relative to the beam axis, and then we simplify the results for the case in which the sphere center is at the beam axis.

A. Sphere not Centered on the Beam Axis

Consider the forces generated by a ray whose beam axis is offset from the microsphere center by a distance d, as shown in Fig. 2. The beam waist is located at the origin O_1 of the rectangular coordinate system with the beam axis away from the z axis that passes through the center of the microsphere. Here, without loss of generality, we assume the beam axis ($\overline{CA}$) passes through the x axis and that the beam waist is located to the left of the microsphere, while the beam is propagating from the left to the right. A ray ($\overline{CP}$) hitting the particle at point P appears to come from a source point at C behind the beam waist. The radius of curvature of this ray is given by

$$R_c = z_p\left[1 + \left(\frac{\rho}{z_p}\right)^2\right] = z_p\left[1 + \left(\frac{\pi n_1 w_o^2}{\lambda_o z_p}\right)^2\right], \quad (4)$$

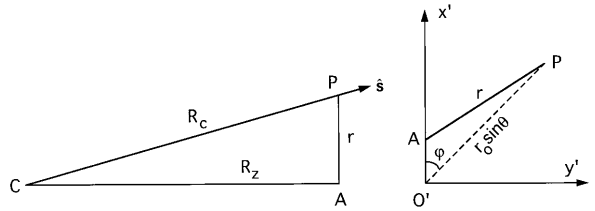

Fig. 3. Geometry of the plane of incidence, showing the direction of the scattering force $\hat{\mathbf{s}}$, and the definition of the distance r from the beam axis to the small region hit by the ray.

where $\rho = \pi n_1 w_o^2/\lambda_o$ is the Rayleigh range in medium n_1, λ_o is the free-space wavelength, and z_p is the z coordinate of point P. Note that the value of R_c can be either positive or negative depending on the sign of z_p; $R_c > 0$ ($R_c < 0$) corresponds to the situation in which w_o is located to the left (right) of the microsphere. The scattering- and the gradient-force components produced by this ray are given by Eqs. (1)–(3), where the unit vectors $\hat{\mathbf{s}}$ and $\hat{\mathbf{g}}$ are determined based on the geometries in Figs. 3 and 4, respectively, as

$$\hat{\mathbf{s}} = [\hat{\mathbf{x}}(r_o \sin\theta \cos\varphi - d) + \hat{\mathbf{y}}(r_o \sin\theta \sin\varphi) + \hat{\mathbf{z}}R_z]/|R_c|, \quad (5a)$$

$$\hat{\mathbf{g}} = (R_c \tan\gamma)^{-1}\left\{\hat{\mathbf{x}}\left(r_o \sin\theta \cos\varphi - d + \frac{dR_c}{a\cos\gamma}\right) + \hat{\mathbf{y}}(r_o \sin\theta \sin\varphi) + \hat{\mathbf{z}}\left[R_z - \frac{R_c(R_z + r_o\cos\theta)}{a\cos\gamma}\right]\right\}. \quad (5b)$$

The details of the calculation of these unit vectors and of the incidence angle α_i are given in Appendix A. Other quantities in Eq. (3) are given by

$$w^2 = w_o^2[1 + (z_p/\rho)^2],$$
$$r^2 = d^2 + (r_o \sin\theta)^2 - 2dr_o \sin\theta \cos\varphi,$$
$$dS = r_o^2 \sin\theta \, d\theta \, d\varphi. \quad (6)$$

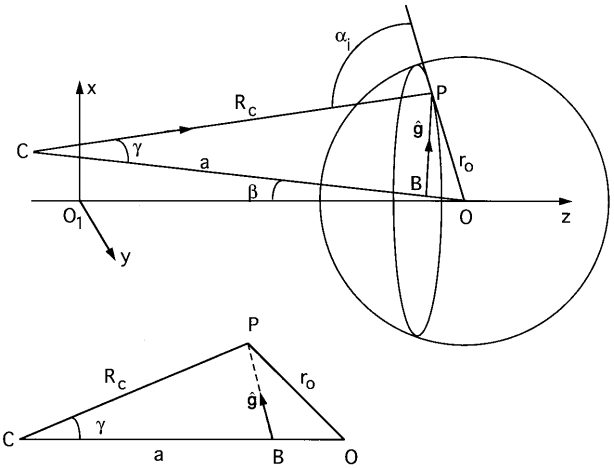

Fig. 4. Geometry of the plane of incidence, showing the direction of the gradient-force $\hat{\mathbf{g}}$.

Because of the spherical symmetry of the problem, the force components $d\mathbf{F}_x$ and $d\mathbf{F}_z$ produced at $P(x_p, y_p, z_p)$ and at $P'(x_p, -y_p, z_p)$ will add up, but the force components $d\mathbf{F}_y$ produced at these two locations will cancel each other. Therefore the total force does not have a y component. Also, when we calculate the other two components of the total force, F_x and F_z, symmetry dictates that the integral with respect to φ need only be carried out from $\varphi = 0$ to $\varphi = \pi$ while we multiply each of the two force components by a factor of 2. Hence the total force produced by the entire beam is

$$\mathbf{F} = \frac{n_1 P_o}{c}\frac{4r_o^2}{\pi}\int_0^{\pi} d\varphi \int_0^{\theta_{\max}} d\theta \sin\theta \times \cos\theta\,(\hat{\mathbf{s}}q_s + \hat{\mathbf{g}}q_g)\frac{\exp(-2r^2/w^2)}{w^2}, \tag{7}$$

with y components of both $\hat{\mathbf{s}}$ and $\hat{\mathbf{g}}$ set to zero. The expression needed to determine the other integral upper limit, $\theta_{\max}$, is also given in Appendix A.

Using Eq. (7), we evaluate the axial and the transverse forces in terms of the corresponding trapping efficiency factors, Q_z and Q_x. They are defined by

$$F_z = \frac{n_1 P_o}{c} Q_z, \tag{8a}$$

$$F_x = \frac{n_1 P_o}{c} Q_x, \tag{8b}$$

in which

$$Q_z = \frac{2r_o^2}{\pi}\int_0^{\pi} d\varphi \int_0^{\theta_{\max}} d\theta \sin 2\theta \frac{\exp(-2r^2/w^2)}{w^2 R_c} \times \left\{ q_s R_z + \frac{q_g}{\tan\gamma}\left[R_z - \frac{R_c(R_z + r_o\cos\theta)}{a\cos\gamma}\right]\right\}, \tag{9a}$$

$$Q_x = \frac{2r_o^2}{\pi}\int_0^{\pi} d\varphi \int_0^{\theta_{\max}} d\theta \sin 2\theta \frac{\exp(-2r^2/w^2)}{w^2 R_c} \times \left\{ q_s(r_o\sin\theta\cos\varphi - d) + \frac{q_g}{\tan\gamma} \times \left[r_o\sin\theta\cos\varphi - d\left(1 - \frac{R_c}{a\cos\gamma}\right)\right]\right\}. \tag{9b}$$

These two expressions are the main results of our analysis. They apply to both circularly polarized and linearly polarized incident beams. For a circularly polarized incident beam, each of R and T in Eqs. (2) must be replaced by its average value, $R_{\text{av}} = (R_{\text{TE}} + R_{\text{TM}})/2$ or $T_{\text{av}} = (T_{\text{TE}} + T_{\text{TM}})/2$, where the subscript av means average and the subscripts TE and TM indicate TE (s) and TM (p) polarization, respectively.[5,6] Alternatively, each of q_s and q_g can be so averaged.[8] The difference arising from these two different choices is negligibly small. For the incident beam that is linearly polarized, however, one first calculates each of Q_z and Q_x for each of TE and TM polarization separately, then adds the contribution from each polarization. In this case, in addition to using the appropriate values for R and T in Eqs. (2), one must also multiply the integrands in Eqs. (9) by a factor of f_s or f_p that corresponds to the fraction of the input power carried by the TE or TM component. These factors are derived in Appendix B.

B. Sphere Centered on the Beam Axis

In a multiple-beam trap, for example, a cross-hair four-beam trap in which four beams propagate toward a center, making an angle of 90° between two adjacent beams, and in an axially aligned, counterpropagating dual-beam trap, the symmetry axis of the beams always passes through the center of the sphere when the sphere is trapped. Therefore we address the particular case of $d = 0$ in this subsection. In this case, due to the azimuthal symmetry, the transverse force component F_x vanishes, and Eq. (9a) reduces to

$$Q_z = 2r_o^2\int_0^{\theta_{\max}} d\theta \sin 2\theta \frac{\exp(-2r^2/w^2)}{w^2} \times (q_s\cos\gamma - q_g\sin\gamma) = 2r_o^2\int_0^{\theta_{\max}} d\theta \sin 2\theta \frac{\exp(-2r^2/w^2)}{w^2 R_c} \times (q_s R_z - q_g r_o\sin\theta), \tag{10}$$

and the angle of incidence is determined from

$$\alpha_i = \cos^{-1}\left[\frac{R_z\cos\theta - r_o\sin^2\theta}{R_c}\right] = \gamma + \theta, \tag{11}$$

where γ is the half-apex angle of the beam and is given by $\gamma = \sin^{-1}(r_o\sin\theta/R_c)$ ($\gamma < 0$ when $R_c < 0$). Equation (11) applies to both $R_c > 0$ (the sphere is located to the left of the beam waist) and $R_c < 0$ (the sphere is located to the right of the beam waist). After substitution of q_s, q_g from Eq. (2) and γ from Eq. (11) into Eq. (10), Q_z reduces to[10]

$$Q_z = 2r_o^2\int_0^{\theta_{\max}} d\theta \sin 2\theta \frac{\exp(-2r^2/w^2)}{w^2} q_z, \tag{12}$$

in which

$$q_z = \cos(\alpha_i - \theta) + R\cos(\alpha_i + \theta) - T^2\frac{\cos(\alpha_i + \theta - 2\alpha_r) + R\cos(\alpha_i + \theta)}{1 + R^2 + 2R\cos 2\alpha_r}. \tag{13}$$

In a fiber-optic trap a situation can be encountered in which r_o is comparable with w_o and $z \gg w_o$. (The particle is located far from each of the beam waists.) In this case the intensity of the trapping beams is approximately constant over the surface area of the microsphere illuminated by the beam, and the beams

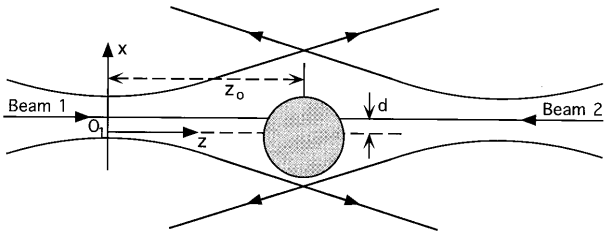

Fig. 5. Geometry of counterpropagating dual Gaussian beams illuminating a dielectric sphere.

are paraxial; that is, $\alpha_i \approx \theta$ and $\gamma \approx 0$, and Eq. (12) reduces to

$$Q_z \approx \frac{2r_o^{\,2}/w_o}{1 + (z_o/\rho)^2} \int_0^{\pi/2} \mathrm{d}\theta q_s \sin 2\theta. \qquad (14)$$

Note that the integral in this expression is independent of z_o. An approximation similar to this has been used in Ref. 3 to evaluate the spring constant corresponding to a dual-fiber trapping force.

C. Dual-Beam, Light-Force Trap

A four-beam trap consists of two orthogonally aligned counterpropagating two-beam traps, each of which itself is a simplest multiple-beam trap. The properties of a four-beam trap can be deduced from a detailed understanding of a two-beam trap. Therefore we examine in detail the performance of a two-beam optical trap as shown in Fig. 5. For this trap the total axial force component F_{zt} and the total transverse force component F_{xt} are

$$F_{zt} = F_{z1} - F_{z2} = \frac{n_1}{c}(P_1 + P_2)Q_{zt}$$
$$= \frac{n_1}{c}(P_1 + P_2)\left(\frac{P_1}{P_1 + P_2}Q_{z1} - \frac{P_2}{P_1 + P_2}Q_{z2}\right), \qquad (15a)$$

$$F_{xt} = F_{x1} + F_{x2} = \frac{n_1}{c}(P_1 + P_2)Q_{xt}$$
$$= \frac{n_1}{c}(P_1 + P_2)\left(\frac{P_1}{P_1 + P_2}Q_{x1} + \frac{P_2}{P_1 + P_2}Q_{x2}\right). \qquad (15b)$$

The subscripts 1 and 2 denote the quantities corresponding to beam 1 and beam 2, respectively. It is clear from these equations that, if the axial and the transverse forces of each beam are comparable, then $F_{xt} \gg F_{zt}$ when $P_1 \approx P_2$. In our numerical analysis we evaluate the total axial and the total transverse trapping efficiency factors Q_{zt} and Q_{xt} defined above. Note that when calculating Q_{z2} and Q_{x2} of beam 2, z_o must be replaced by $s - z_o$, where s is the spacing between the waists of the two beams.

3. Numerical Results

In this section numerical examples are presented for a dual-beam fiber-optic light-force trap. Q_{zt} and Q_{xt} are evaluated for a range of values of the normalized parameters, including the beam waist separation distance $S = s/w_o$, the microsphere radius $R_o = r_o/w_o$, and the effective refractive index $N = n_2/n_1$, where n_2 is the index of refraction of the dielectric microsphere. The case of circularly polarized input beams is analyzed first. In such cases, following Roosen and coworkers,[5,6] each R and T is calculated as the average of that corresponding to TE polarization and that corresponding to TM polarization, respectively, for each illuminated element of the sphere. Then transverse trapping efficiency corresponding to circularly polarized input beams is compared with that corresponding to linearly polarized beams, and the performance of a lensed fiber-optic trap is compared with that of a cleaved-fiber trap. The normalized wavelength in medium n_1, $\Lambda = (\lambda_o/n_1)/w_o$, is fixed at a value of $\Lambda = 0.15$. (This approximately corresponds to a laser beam with $w_o = 5$ μm and $\lambda_o = 1.064$ μm and a microsphere suspended in water with $n_1 = 1.33$.) This gives an asymptotic half-apex angle of $\theta_{\text{beam}} \approx (\lambda_o/n_1)/\pi w_o = 8.6°$ for the beam in the suspending medium. In all the calculations presented below, the power P_o, the wavelength λ_o, and the beam waist w_o are assumed to be the same for both fibers.

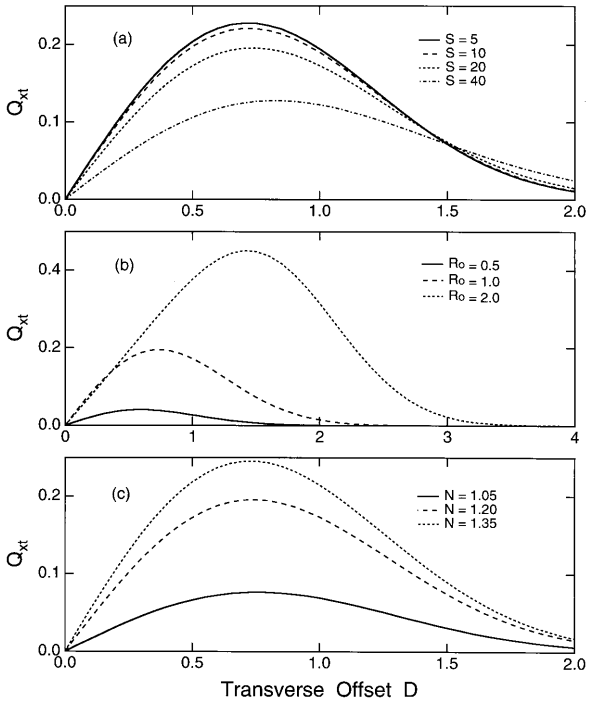

Fig. 6. Variation of the transverse trapping efficiency Q_{xt} as a function of the transverse offset D with (a) the beam waist separation S, (b) the sphere radius R_o, and (c) the effective index of refraction N as a parameter. Parameters not shown in the legends are $S = 30$, $R_o = 1$, and $N = 1.2$.

A. Transverse Trapping Force

The dependence of the transverse trapping efficiency Q_{xt} on the transverse offset $D = d/w_o$ is shown for different values of beam waist spacing, microsphere radius, and effective refractive index in Figs. 6(a), 6(b), and 6(c), respectively. In each case Q_{xt} is calculated at $Z_o = z_o/w_o = S/2$, where $Q_{zt} = 0$. When

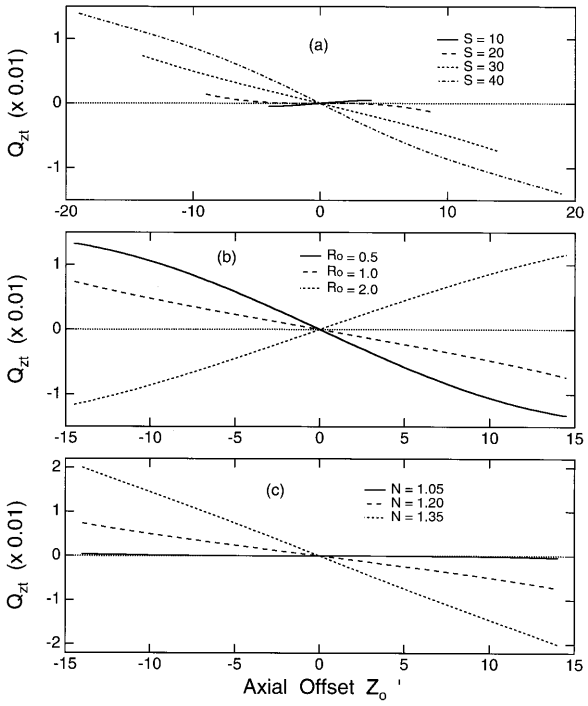

Fig. 7. Same as Fig. 6, except that the axial trapping efficiency Q_{zt} is plotted versus the axial offset $Z_o' = Z_o - S/2 = z_o/w_o - S/2$.

not indicated in the legends of the figures, the parameter values $S = 20$, $R_o = 1$, and $N = 1.2$ are used. When R_o and N are fixed, the total light power intercepting the sphere decreases with increasing S; therefore the slope and the maximum value of Q_{xt} also decrease [Fig. 6(a)]. When R_o is increased, more beam power illuminates the sphere; thus the maximum value of the transverse force increases. The slope of the Q_{xt} curve grows in the interval $R_o =$ 0.5–1 with R_o; after that it stays almost constant. When N is varied both the peak value and the slope of Q_{xt} increase with N [Fig. 6(c)] owing to the greater change in the input beam momentum. That is, a shorter beam waist spacing, a larger particle dimension, and a larger effective index of refraction result in more stable transverse confinement of the particle. But, for a given beam waist, making the fiber spacing smaller and choosing particles with larger diameters may not favor increasing the axial stability or, in the worse case, may not even produce a point of stable equilibrium, as is shown in the next subsection.

B. Axial Trapping Force

Figures 7(a), 7(b), and 7(c) show the axial trapping efficiency Q_{zt} as a function of the shifted axial offset

$$Z_o' = Z_o - S/2 = z_o/w_o - S/2, \tag{16}$$

for varying beam waist spacing S, microsphere radius R_o, and effective index of refraction N, respectively. These calculations are performed for microspheres centered on the beam axis ($D = 0$); therefore $Q_{xt} = 0$. The parameters not indicated in the legends of these figures are $S = 30$, $R_o = 1$, and $N = 1.2$. In each case

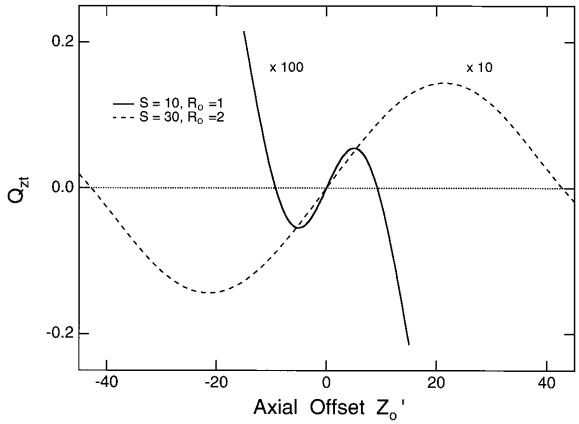

Fig. 8. Variation of the axial trapping efficiency Q_{zt} as a function of the axial offset Z_o' when $N = 1.2$.

the force is calculated only for $Z_o > 0$, that is, within the beam waist spacing of the two beams. A general observation is that the maximum value of the axial efficiency Q_{zt} is smaller than that of the transverse efficiency Q_{xt} (Fig. 6) by at least an order of magnitude. When the beam waist spacings are large, such as $S = 20$, 30, 40 of Fig. 7(a), the trapping efficiency exhibits a region of linear restoring force in the vicinity of $Z_o' = 0$. In the case of microlensed fibers, the radius of each beam becomes minimum at a certain distance from the fiber end, and Q_{zt} exhibits nonlinear behavior in the region between each fiber end and the minimum beam radius,[11] which is not shown here. When the beam waist spacing is decreased, the axial distance over which Q_{zt} remains linear decreases, eventually reaching a limit at which the slope of Q_{zt} becomes zero. As S is decreased beyond this limit, Q_{zt} possesses a positive slope, as displayed by the $S = 10$ curve in Fig. 7(a). In this case the position $Z_o' = 0$ corresponds to a point of unstable equilibrium. In the case of cleaved fibers the particle will be trapped against the end face of one of the fibers. If the fibers have microlenses at their end faces, then the axial trapping force exhibits two stable equilibrium points, each between a fiber end and the corresponding beam waist. This situation is further explained in Fig. 8, where Q_{zt} is replotted for the case of $S = 10$ (the solid curve) as Z_o is varied from -10 to 20. (The beam waists are located at $Z_o' = \pm 5$.) Such a bistable behavior has been experimentally observed by Lyons and Sonek.[11] The slope of Q_{zt} increases with increased effective index of refraction [Fig. 7(c)] as does the slope of Q_{xt} curve. But, in contrast to the transverse trapping efficiency, the slope of Q_{zt} decreases with decreased beam waist spacing and increased sphere radius [Figs. 7(a) and 7(b)]. This can be understood from Fig. 9, where Q_{z1} is plotted versus Z_o for the parameters used in Fig. 7(b) and for an additional case of $R_o = 1.5$. When $R_o < 1$, Q_{z1} decreases monotonically with Z_o, since in this case the input laser beam increasingly overfills the microsphere with decreased intensity. But, when $R_o \geq 1$, it increases first and then decreases,

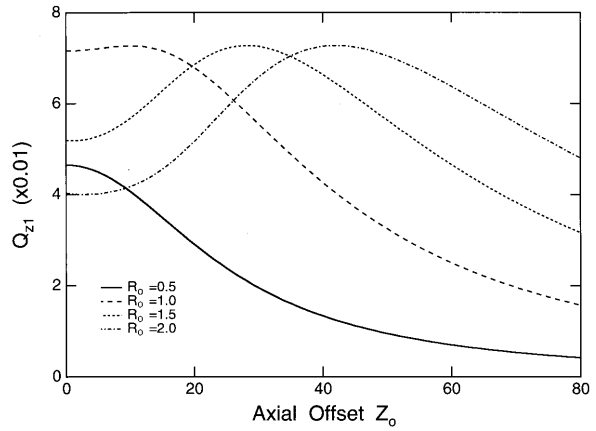

Fig. 9. Variation of the axial trapping efficiency Q_{z1} of beam 1 (Fig. 5) as a function of the axial offset Z_o when $N = 1.2$.

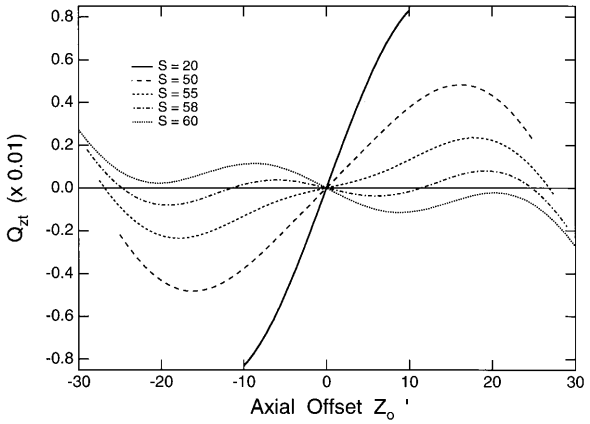

Fig. 10. Variation of the axial trapping efficiency Q_{zt} as a function of the axial offset Z_o' when $R_o = 1.5$ and $N = 1.2$.

since the laser beam underfills the particle when the particle is close to the fiber end and overfills it with a much reduced intensity when the particle is moved too far from the fiber. We found numerically that for $R_o \geq 1.5$, the value $Z_o = Z_{\max}$ at which Q_{z1} becomes a maximum under the conditions of Fig. 9 is related to R_o by $Z_{\max} \approx 26R_o - 10.5$. The negative slope of Q_{zt} becomes larger when one chooses $Z_o = S/2$ in which Q_{z1} has larger negative slope. If S is chosen such that at $Z_o = S/2$ the Q_{z1} curve has a positive slope, then the Q_{zt} curve will also have a positive slope, as shown in Fig. 7(b) by the $R_o = 2$ curve. In this case the central equilibrium point is again unstable, but the force has two stable equilibrium points located at $Z_o' \approx \pm 43$ (each of which is between one fiber end face and the nearer beam waist in a microlensed fiber trap), as shown by the dashed curve in Fig. 8.

In the examples presented above, the bistable behavior of the axial force is predicted only for traps with lensed fibers. However, such a behavior of the axial force is not limited to lensed fibers. When the sphere radius is greater than the beam waist, at a certain range of beam waist spacings, the axial force can exhibit multiple points of stable equilibrium even in traps with cleaved optical fibers or within the distance of the two beam waists. This is shown by the example in Fig. 10. In this figure Q_{zt} is plotted versus Z_o' for $R_o = 1.5$, $N = 1.2$, and for several values of S. In this particular case two stable and one unstable equilibrium points exist when $S = 55$, and three stable and two unstable equilibrium points exist when $S = 58$, within the waists of the two beams. Although only one special case of $R_o = 1.5$ is examined in this example, we found that this situation is rather general for large R_o. This can also be understood from Fig. 9. When R_o is large, the axial force of each fiber first increases and then decreases with the axial distance, but at different rates. Therefore within a certain range of fiber spacing, the axial forces of the two counterpropagating beams become equal in several axial positions and result in several points of stable and unstable equilibrium.

We have also examined the applicable range of the approximate expression of Q_z given by relation (14). We found that to achieve acceptable accuracy in approximate Q_z calculations, S must be fairly large. For example, when $N = 1.2$ and $S = 50$, the errors in the Q_z value obtained from relation (14) relative to that obtained from Eq. (12) are $\{5, 22, 125\}\%$ for $R_o = \{0.5, 1, 2\}$, respectively.

C. Polarization Effects

When the microsphere is located on the beam axis, both a circularly polarized beam and a linearly polarized beam produce the same amount of axial force, and, as was discussed above, the transverse force vanishes. However, when the microsphere is located at a distance d from the beam axis, there is some difference in both components of the forces produced by a circularly polarized beam and by a linearly polarized beam. To investigate the effects of different states of polarization, we calculated Q_{xt} as a function of D for a special case of $S = 20$, $R_o = 1$, $N = 1.2$, and for three different cases of polarization. The results are shown in Fig. 11, where the solid curve corresponds to a circularly polarized beam, and the long-dashed and short-dashed curves correspond to the beams linearly polarized in the x and the y directions, respectively. As in the case of single-beam gradient trap,[8] the differences in forces resulting from these different choices of input beam polarization are not large. In the particular case of Fig. 11, the difference of the forces that resulted from the input beams polarized in the x and the y directions increases monotonically with D until $D \approx 2$, reaching a maximum of 14% at $D = 2$. Therefore it is quite reasonable to calculate the transverse force assuming a circularly polarized input beam; the resulting force is close to the average of the forces of the beams polarized in the x and the y directions, respectively.

D. Roles of Microlenses

Employing microlenses in a counterpropagating two-beam trap is expected to enhance the trapping stability and to increase the trapping volume.[11] To

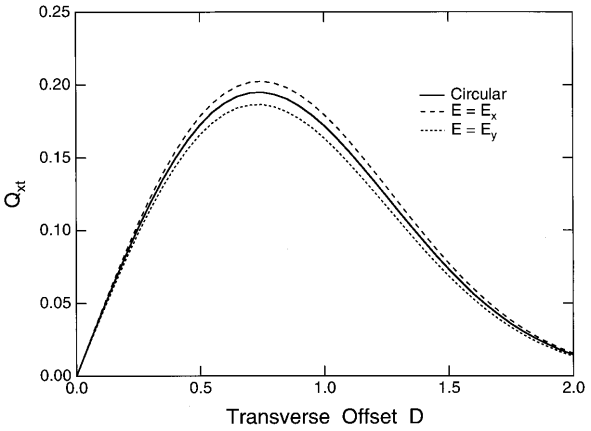

Fig. 11. Dependence of the transverse trapping efficiency Q_{xt} on the state of incident beam polarization. The solid curve is for a circularly polarized beam, and the long- and the short-dashed curves are for the beams linearly polarized in the x and the y directions, respectively. Other parameters are $S = 20$, $R_o = 1$, and $N = 1.2$.

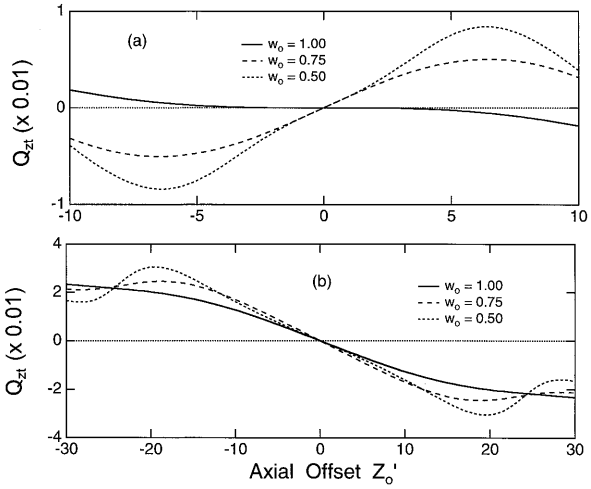

Fig. 13. Dependence of the axial trapping efficiency Q_{zt} on the waist of incident beam when (a) $S = 20$ and (b) $S = 60$. Other parameters are $r_o = 1$ and $N = 1.2$.

explore the advantages of microlenses, we calculated the transverse and the axial forces for focused Gaussian beams. We considered three different values for the normalized beam waist w_o and two values for beam waist spacing, $S = 20$ and $S = 60$. The results of Q_{xt} and Q_{zt} are shown in Figs. 12 and 13, respectively. When $S = 20$, reducing w_o indeed improves the stiffness of the transverse force [Fig. 12(a)], but slightly decreases the trapping volume and, in this particular case, weakens and even loses the stability of the axial force [Fig. 13(a)]. When $S = 60$, decreasing w_o increases the trapping volume slightly but greatly weakens the transverse stability [Fig. 12(b)], and the improvement in the axial stability is not so meaningful either [Fig. 13(b)]. The changes that a decreased w_o introduces on the transverse stability can be understood from the corresponding changes in the beam field radius as shown in Fig. 14, where the beam field radius is plotted versus the axial offset Z_o for the same three values of w_o. When $S = 20$, the beam radius at the axial equilibrium plane (which corresponds to $Z_o = 10$ in Fig. 14) decreases with decreased w_o and results in a smaller trapping volume. When $S = 60$, although the beam field radius increases with decreased w_o in the plane of axial equilibrium ($Z_o = 30$), the power density of the beam is greatly reduced, resulting in a slightly improved trapping volume but significantly reduced transverse stiffness. The analysis of these two cases illustrate that using microlenses in a dual-fiber trap does not necessarily increase both the trapping stability and the trapping volume simultaneously.

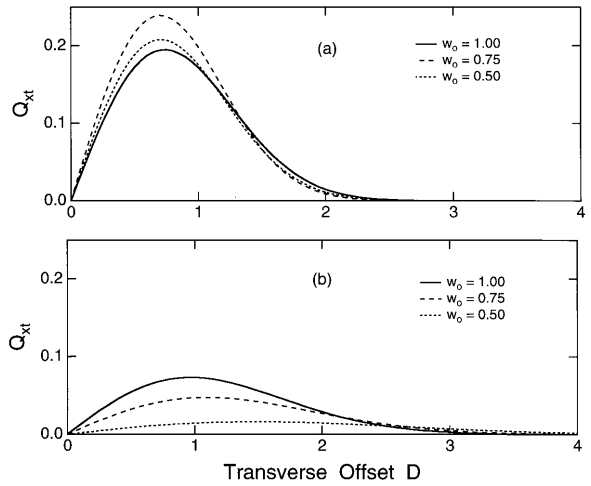

Fig. 12. Dependence of the transverse trapping efficiency Q_{xt} on the waist of incident beam when (a) $S = 20$ and (b) $S = 60$. Other parameters are $r_o = 1$ and $N = 1.2$.

4. Comparison of Counterpropagating Dual-Beam Traps and Gradient-Force Traps

The calculations described in the previous section show that the magnitudes of the transverse and the axial forces produced by a Gaussian beam on a dielectric microsphere can have a big difference, the

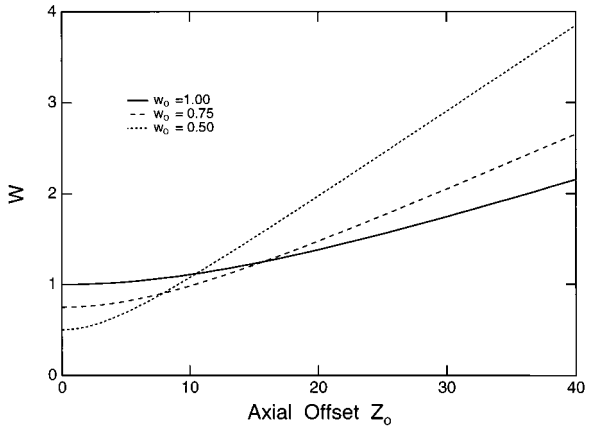

Fig. 14. Dependence of beam field radius $W = w/w_o$ on the beam waist.

transverse force being larger than the axial force by more than an order of magnitude. Therefore in a counterpropagating two-beam fiber-optic trap the axial stability is always much lower than the transverse stability, as was observed experimentally by Constable *et al.*[3] Also, fiber spacing must be larger than a certain limit to produce a stable point of equilibrium, and there can be more than one stable point of equilibrium within the spacing of the two fibers. Combining several counterpropagating dual-beam fiber-optic traps results in a new trap: the fiber-optic gradient-force trap. A simplest example is a four-beam trap, in which four optical fibers are positioned perpendicular to each other such that the four beams emerging from these fibers form a cross hair at their common intersection. In such a trap the three-dimensional confinement of the microsphere is solely by transverse forces; therefore this trap provides much stronger stability or requires much less laser power as compared with a dual-fiber counterpropagating beam trap. The magnitude and the stiffness of the trapping forces are comparable with those obtained in single-beam optical tweezers.[2] There is only one stable point of equilibrium located at the beam-crossing center of the trap, and there is no limit for the minimum fiber spacing as well. A particle can be trapped with only two or three beams launched from adjacent fibers, or it can be manipulated in a plane by adjustment of the individual light beam intensities. Therefore fiber-optic gradient-force traps possess great advantages over the counterpropagating two-beam traps.

According to the results presented in subsection 3.D, the use of microlenses in a four-beam gradient-force trap will improve the stability of the trap only if the spacing between each pair of axially aligned fibers is sufficiently small, but this may lose some manipulative capabilities of the trap as well, as discussed in Subsection 3.D.

5. Discussion and Conclusions

A comprehensive analysis has been presented of transverse and axial forces exerted on a dielectric sphere by two counterpropagating laser beams in a dual-beam optical trap, accounting for the off-axis location of the sphere relative to the symmetry axis of the laser beam and the axial divergence of the laser beam. The analysis is applicable to dual-beam optical traps with either unfocused (e.g., emerging from bear fibers) or weakly focused (e.g., emerging from microlensed fibers or from two lenses if the trap employs a conventional microscope) Gaussian beams, to multiple-beam fiber-optic gradient-force traps, and to single-beam gradient traps with tightly focused laser beams.[10] The ray optics approach employed in this analysis is highly accurate in predicting both axial and transverse forces in the particle size regime $r_o \geq 10\lambda_o$ (Ref. 8) and can still give reasonable predictions for spheres with $r_o < 10\lambda_o$, especially for multiple-beam traps with unfocused or weakly focused beams delivered by optical fibers.

Multiple-beam fiber-optic light-force traps have been investigated theoretically. It was found that, for a given beam waist and a fixed wavelength, the maximum value and the slope of the transverse force increase with decreased beam waist spacing, increased sphere size, and increased effective index of refraction. The maximum value and the slope of the axial force also increase with increased effective index of refraction, but the axial force exhibits different regimes of stable equilibrium when beam waist spacing and sphere size are varied. In particular, when the sphere radius is greater than the beam waist, axial force can exhibit as many as three points of stable equilibrium within the spacing of the two beam waists, which is a new discovery of this study. To realize a single point of stable equilibrium within the two beam waists in a counterpropagating dual-beam trap, the beam waist spacing must be made larger than a certain limit that is determined by the relative values of the beam waist and the particle radius. Effects of different states of polarization of the input electric field and the functions of the microlenses attached to the fibers have been examined. It was found that different polarization states do not introduce large differences in the trapping forces; therefore for good approximation, the force components can be calculated assuming a circularly polarized input beam. For a dual-beam fiber-optic trap the use of microlenses does not produce any practical advantage in terms of its trapping stability and trapping volume.

A four-beam fiber-optic trap can be used as a two-beam, a three-beam, or a four-beam gradient-force trap when light is injected into different groups of fibers. In such a trap the forces confining a particle are all gradient forces, which are much stronger than the scattering forces, are almost the same in all directions, and are comparable with those obtainable in a single-beam gradient trap. Therefore the fiber-optic gradient-force traps provide greatly enhanced stability as compared with the corresponding counterpropagating dual-beam traps.

Appendix A: Unit Vector along the Axial and the Transverse Forces and the Angle of Incidence

Consider the forces generated by a ray hitting the sphere at point P offset from the center of the sphere by a distance d (Fig. 2). The three coordinates $\{x_p, y_p, z_p\}$ of point P (situated above the page's plane) are given in terms of the spherical coordinates by

$$\begin{aligned} x_p &= r_o \sin\theta \cos\varphi, \\ y_p &= r_o \sin\theta \sin\varphi, \\ z_p &= z_o - r_o \cos\theta, \end{aligned} \tag{A1}$$

where r_o is the radius of the particle, z_o is the z coordinate of the microsphere center, and $\pi - \theta$ and φ are the polar and the azimuthal angles in spherical coordinates, respectively. The unit vector $\hat{\mathbf{s}}$ is determined on the basis of the geometry in Fig. 3. The

three coordinates $\{x_c, y_c, z_c\}$ of point C are

$$x_c = d,$$
$$y_c = 0,$$
$$z_c = -[R_z - (z_o - r_o \cos\theta)], \quad \text{(A2)}$$

where R_z is the projection of vector **CP** onto the z axis and is given by

$$R_z = \pm(R_c^2 - r^2)^{1/2}. \quad \text{(A3)}$$

Here the plus (minus) sign should be chosen when $R_c > 0$ ($R_c < 0$). $\hat{\mathbf{s}}$ is defined as

$$\hat{\mathbf{s}} = [\hat{\mathbf{x}}(x_p - x_c) + \hat{\mathbf{y}}(y_p - y_c) + \hat{\mathbf{z}}(z_p - z_c)]/|R_c|, \quad \text{(A4)}$$

where $\{\hat{\mathbf{x}}, \hat{\mathbf{y}}, \hat{\mathbf{z}}\}$ are the unit vectors along the three axes in the rectangular coordinate system. Substituting Eqs. (A1) and (A2) into Eq. (A4) yields Eq. (5a).

As is shown in Fig. 4, the extension of the unit vector $\hat{\mathbf{g}}$ intersects $\overline{CO} = a$ (which lies in the xz plane) at point B. To determine $\hat{\mathbf{g}}$, we first need to determine the three coordinates $\{x_b, y_b, z_b\}$ of this point B. For triangle CPO we have $r_o^2 = R_c^2 + a^2 - 2aR_c \cos\gamma$, from which we obtain

$$\gamma = \cos^{-1}\left(\frac{R_c^2 + a^2 - r_o^2}{2aR_c}\right), \quad \text{(A5)}$$

where

$$a = [d^2 + (R_z + r_o \cos\theta)^2]^{1/2}. \quad \text{(A6)}$$

From the right triangle CPB we have $\cos\gamma = R_c/(a - \overline{OB})$ or $\overline{OB} = a - R_c/\cos\gamma$, from which we obtain

$$x_b = \overline{OB}\sin\beta = d\left(1 - \frac{R_c}{a\cos\gamma}\right),$$
$$y_b = 0,$$
$$z_b = z_o - \overline{OB}\cos\beta = z_o - \left(1 - \frac{R_c}{a\cos\gamma}\right)(R_z + r_o\cos\theta). \quad \text{(A7)}$$

The unit vector $\hat{\mathbf{g}}$ is defined as

$$\hat{\mathbf{g}} = [\hat{\mathbf{x}}(x_p - x_b) + \hat{\mathbf{y}}(y_p - y_b) + \hat{\mathbf{z}}(z_p - z_b)]/\overline{PB}, \quad \text{(A8)}$$

where $\overline{PB} = R_c \tan\gamma$ is the distance between points B and P. Substituting the expressions of $\{x_p, y_p, z_p\}$ and $\{x_b, y_b, z_b\}$ from Eqs. (A1) and (A7) into Eq. (A8) yields Eq. (5b).

We also need to derive an expression for the incidence angle α_i. From Fig. 4, $a = \overline{CO}$ can also be written as

$$a^2 = r_o^2 + R_c^2 - 2r_oR_c\cos(\pi - \alpha_i). \quad \text{(A9)}$$

Combining this with Eq. (A6) yields

$$\alpha_i = \cos^{-1}\left[\frac{d^2 + (R_z + r_o\cos\theta)^2 - r_o^2 - R_c^2}{2r_oR_c}\right]. \quad \text{(A10)}$$

This expression applies when the beam focus is located either to the left or to the right of the sphere. The angle of refraction α_r is determined from Snell's law. For each given value of φ, the boundary of the illuminated part of the microsphere is determined by θ_{max}, which is obtained from the condition $\alpha_i = \alpha_{max} = \pi/2$. From Eq. (A9), this upper limit θ_{max} of θ can be determined numerically by solution of

$$d^2 + (R_z + r_o\cos\theta)^2 - r_o^2 - R_c^2 = 0 \quad \text{(A11)}$$

with $\theta = \theta_{max}$.

Appendix B: Effects of Linear Polarization: f_s and f_p

We now derive expressions for the factors f_s and f_p. In Fig. 2 the plane of incidence passes through three points, O, P, and C, in space. Using the three coordinates of each of these points given by Eqs. (A1) and (A2) as well as $x_o = y_o = 0$ and $z_o = z_o$, we obtain the following equation for the plane of incidence:

$$Ax + By + Cz + D = 0, \quad \text{(B1)}$$

where

$$A = r_o\sin\theta\sin\varphi(R_z + r_o\cos\theta),$$
$$B = dr_o\cos\theta - r_o\sin\theta\cos\varphi(R_z + r_o\cos\theta),$$
$$C = dr_o\sin\theta\sin\varphi,$$
$$D = dz_or_o\sin\theta\sin\varphi. \quad \text{(B2)}$$

If the polarization is in the x direction, then

$$f_s = \sin^2\phi_x = \frac{A^2}{A^2 + B^2 + C^2}, \quad \text{(B3)}$$

where ϕ_x is the angle between the x axis and the plane of incidence. For the polarization in the y direction,

$$f_s = \sin^2\phi_y = \frac{B^2}{A^2 + B^2 + C^2}, \quad \text{(B4)}$$

in which ϕ_y is the angle between the y axis and the plane of incidence. In both cases

$$f_p = 1 - f_s. \quad \text{(B5)}$$

We acknowledge support for this research from the Whitaker Foundation.

References and Notes

1. A. Ashkin, "Acceleration and trapping of particles by radiation pressure," Phys. Rev. Lett. **24,** 156–159 (1970).
2. A. Ashkin, J. M. Dziedzic, J. E. Bjorkholm, and S. Chu, "Observation of s single-beam gradient force optical trap for dielectric particles," Opt. Lett. **11,** 288–290 (1986).
3. A. Constable, J. Kim, J. Mervis, F. Zarinetchi, and M. Prentiss, "Demonstration of a fiber-optical light-force trap," Opt. Lett. **18,** 1869–1871 (1993).
4. K. Svoboda and S. M. Block, "Biological applications of optical forces," Ann. Rev. Biophys. and Biomol. Struc. **23,** 247–285 (1994).
5. G. Roosen and C. Imbert, "Optical levitation by means of two horizontal laser beams: a theoretical and experimental study," Phys. Lett. A **59,** 6–8 (1976).

6. G. Roosen, "A theoretical and experimental study of the stable equilibrium positions of spheres levitated by two horizontal laser beams," Opt. Commun. **21,** 189–194 (1977).
7. G. Roosen, "La levitation optique de spheres," Can. J. Phys. **57,** 1260–1279 (1979).
8. A. Ashkin, "Forces of a single-beam gradient laser trap on a dielectric sphere in the ray optics regime," Biophys. J. **61,** 569–582 (1992).
9. T. C. B. Schut, G. Hesselink, B. G. Degrooth, and J. Greve, "Experimental and theoretical investigations on the validity of the geometrical optics model for calculating the stability of optical traps," Cytometry **12,** 479–485 (1991).
10. R. Gussgard, T. Lindmo, and I. Brevik, "Calculation of the trapping force in a strongly focused laser beam," J. Opt. Soc. Am. B **9,** 1922–1930 (1992).
11. E. R. Lyons and G. J. Sonek, "Confinement and bistability in a tapered hemispherically lensed optical fiber trap," Appl. Phys. Lett. **66,** 1584–1586 (1995).
12. The directions of $\hat{\mathbf{g}}$ here and in Ashkin's paper (Y axis in Fig. 3 of Ref. 8) are opposite. The value of q_g in Ref. 8, denoted by Q_g, is always less than zero (negative) under the definition given by Eqs. (2) and (3), but Ashkin switches the direction of F_g in his Fig. 2(B) and also plots - Q_g in his Fig. 3. We defined our q_g as $q_g = -Q_g$ and changed the direction of $\hat{\mathbf{g}}$ correspondingly. This is also consistent with the definition in Refs. 5 and 6. Under this definition, when a ray strikes a small region of the surface of a microsphere, the component of the force exerted on the microsphere in the direction perpendicular to the ray axis is such that it pulls the microsphere toward the ray axis, provided that $n_2 > n_1$.
13. We used θ, not α_i as is done in Ref. 10 for the same purpose, because the transverse distribution of the light intensity I given in Eq. (3) is defined in a plane perpendicular to the beam axis, even though the individual rays of the beam hit the microsphere at certain nonzero angles with respect to the beam axis.